

PAPER • OPEN ACCESS

Practical method for analyzing singular index and intensity of singular stress field for three dimensional bonded plate

To cite this article: Tatsujiro Miyazaki *et al* 2018 *IOP Conf. Ser.: Mater. Sci. Eng.* **372** 012002

View the [article online](#) for updates and enhancements.

Related content

- [Evaluation of debonding strength of single lap joint by the intensity of singular stress field](#)
Tatsujiro Miyazaki and Nao-Aki Noda
- [Intensity of singular stress field for three-dimensional butt joint to evaluate the adhesive strength](#)
N-A Noda, K Tsuboi, R Takaki et al.
- [Intensity of singular stress fields of an embedded fibre under pull-out force](#)
D Chen, G W Zhang, R Takaki et al.



IOP | ebooks™

Bringing you innovative digital publishing with leading voices to create your essential collection of books in STEM research.

Start exploring the collection - download the first chapter of every title for free.

Practical method for analyzing singular index and intensity of singular stress field for three dimensional bonded plate

Tatsujiro Miyazaki^{1,4}, Takuma Inoue² and Nao-Aki Noda³

¹University of the Ryukyus, 1 Senbaru, Nishihara-cho, Nakagami-gun, Okinawa 903-0213, Japan

²Graduate School of Engineering and Science, University of the Ryukyus, 1 Senbaru, Nishihara-cho, Nakagami-gun, Okinawa 903-0213, Japan

³Kyushu Institute of Technology, 1-1 Sensui-cho, Tobata-ku, Kitakyushu-shi, Fukuoka 804-8550, Japan

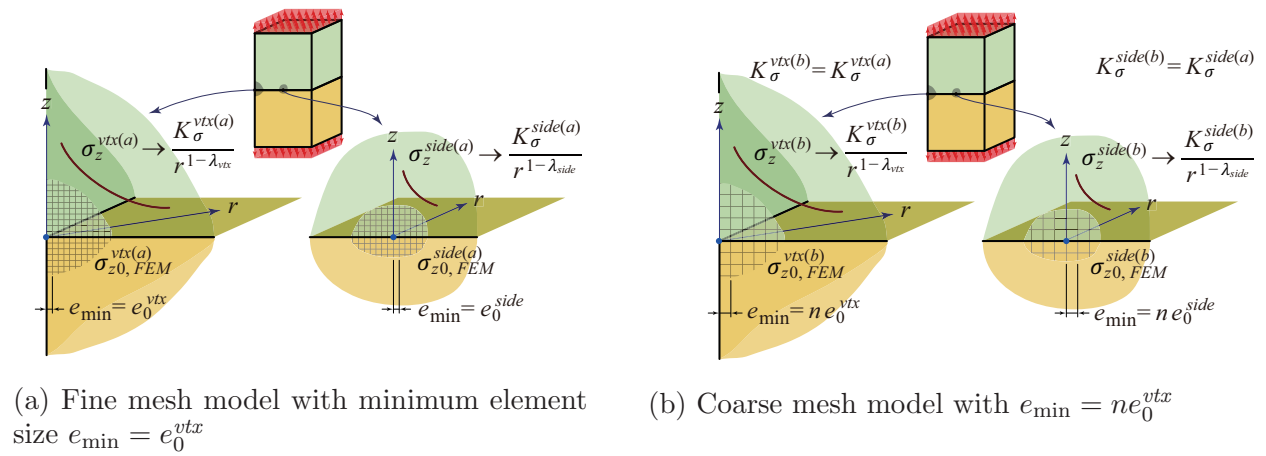
E-mail: t-miya@tec.u-ryukyu.ac.jp

Abstract. In this paper, the practical analysis methods are proposed for analyzing the singular index and the intensity of singular stress field (ISSF) at the vertex of the interface in the three dimensional (3D) bonded plate. The analysis methods focus FEM stresses at and around the vertex. The singular index is determined from the FEM stress ratio at the vertex obtained by performing FEM analyses on the finely and coarsely meshed models. Then, the ISSF is determined by the ratio of the average FEM stresses at and around the vertex obtained by performing the FEM analyses on the reference and unknown models under the same mesh pattern. The validity of the present methods was examined by the plane strain bonded plate and 3D bonded plate in the literature. It was found that the present methods for the singular index have the same accuracy as the FEM eigenvalue analysis. The asymptotic solutions with the singular index and ISSF by the present method correspond to FEM stress distributions. Since the ISSF by the body force method (BFM) is used as the reference solution, the present method for ISSF has the same accuracy as BFM. Moreover, the critical ISSF values were calculated in the experimental results of the butt joints with various adhesive thicknesses. In the case of the ductile epoxy adhesive, it was shown that the critical ISSF at the vertex by 3D model was more constant against the thickness than that by 2D model. The result is quite different from that of the brittle epoxy adhesive and can be never obtained by 2D model.

1. Introduction

The intensity of singular stress field (ISSF) is useful for evaluating the debonding strength [1–4]. Generally, the finite element method (FEM) is often used to evaluate the strength in various industries [5, 6]. However, the ISSF cannot be calculated directly by FEM [7–10]. The authors proposed the method for calculating the ISSF easily and accurately by the FEM [3, 4, 11, 12]. The method does not require the complex calculation and can be applied to various bonded structures. In the previous studies, the ISSF for the butt joint was analyzed by 2D model [3, 4]. It was found that the debonding fracture criterion can be expressed with the ISSF [11, 13]. Actual butt joint has the vertex and its debonding fracture is caused from the vertex of the interface. However, it is difficult to analyze the ISSF at the vertex and the debonding fracture





(a) Fine mesh model with minimum element size $e_{\min} = e_0^{vtx}$ (b) Coarse mesh model with $e_{\min} = n e_0^{vtx}$

Figure 1. Schematic illustration of 3D bonded plate models for analyzing the singular index

criterion is not discussed by the ISSF at the vertex in 3D model.

In this paper, the practical analysis methods are proposed for analyzing the singular index and the ISSF at the vertex of the interface in 3D bonded plate. The critical ISSF values are calculated in the experimental results of the butt joints with various adhesive thicknesses and are compared with those by 2D model.

2. Analysis method for singular index and intensity of singular stress field

2.1. Analysis method for singular index

Figure 1 shows the schematic illustrations of the 3D bonded plate models. The model (a) is subdivided by the minimum element size $e_{\min} = e_0^{vtx}$. The FEM stress in the z direction and the ISSF at the vertex of the interface are denoted with $\sigma_{z0, FEM}^{vtx(a)}|_{e_{\min}=e_0^{vtx}}$ and $K_{\sigma}^{vtx(a)}$, respectively. The model (b) is as large as the model (a) and subdivided by $e_{\min} = n e_0^{vtx}$. The FEM stress in the z direction and the ISSF at the vertex of the interface are denoted with $\sigma_{z0, FEM}^{vtx(b)}|_{e_{\min}=n e_0^{vtx}}$ and $K_{\sigma}^{vtx(b)}$, respectively.

The real singular stress in the z direction at the vertex of the interface in 3D bonded plate is given by the following equation [9].

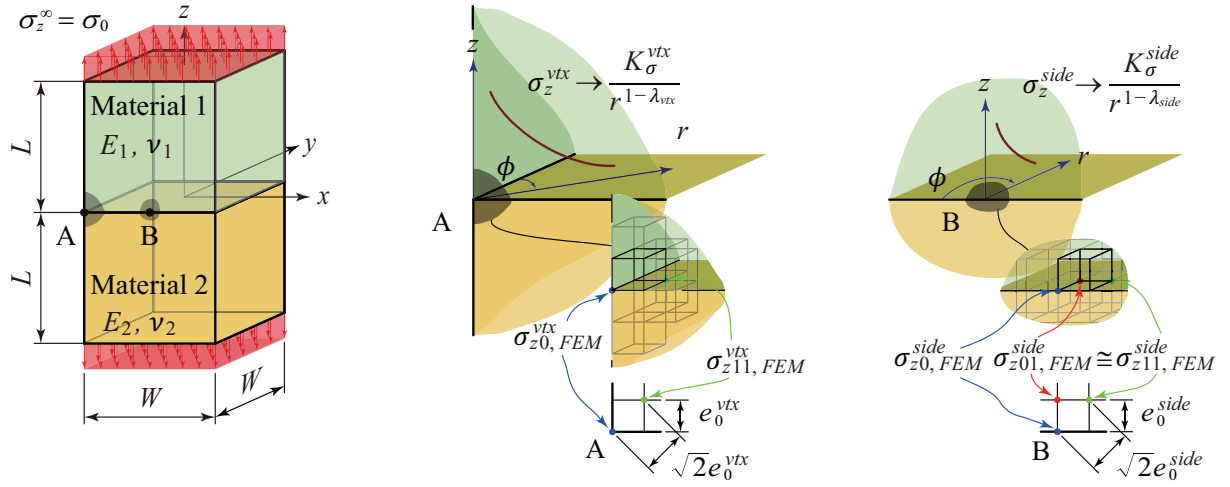
$$\sigma_z^{vtx} = \frac{K_{\sigma}^{vtx}}{r^{1-\lambda_{vtx}}} \quad (1)$$

Here, r is the distance from the vertex, λ is the singular index at the vertex, K_{σ} is the ISSF at the vertex. Since the minimum element size of the model (b) is n times as large as that of the model (a), the relation between the FEM stresses $\sigma_{z0, FEM}^{vtx(a)}|_{e_{\min}=e_0^{vtx}}$ and $\sigma_{z0, FEM}^{vtx(b)}|_{e_{\min}=n e_0^{vtx}}$ can be expressed as follows [11].

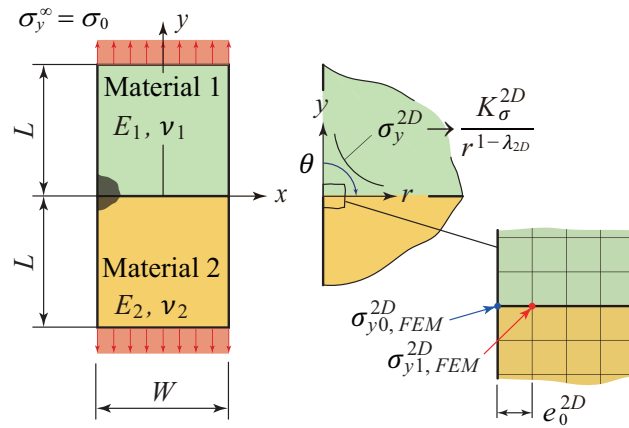
$$\sigma_{z0, FEM}^{vtx(a)}|_{e_{\min}=e_0^{vtx}} \cdot e_0^{1-\lambda_{vtx}} = \sigma_{z0, FEM}^{vtx(b)}|_{e_{\min}=n e_0^{vtx}} \cdot (n e_0^{vtx})^{1-\lambda_{vtx}} = \text{constant} \quad (2)$$

Solving Eq. (2) on λ_{vtx} , the following equation is obtained.

$$\lambda_{vtx} = 1 - \frac{\ln\left(\sigma_{z0, FEM}^{vtx(a)}|_{e_{\min}=e_0^{vtx}} / \sigma_{z0, FEM}^{vtx(b)}|_{e_{\min}=n e_0^{vtx}}\right)}{\ln n} \quad (3)$$



(a) 3D bonded plate model.



(b) 2D bonded plate model.

Figure 2. Schematic illustration of 2D and 3D bonded plate models.

Generally, the finite element eigen analysis method is often used for the analysis of λ_{vtx} . λ_{vtx} can be determined by Eq. (3) much more easily than the finite element eigenanalysis method.

When the FEM stresses $\sigma_{z0,FEM}^{side(a)}|_{e_{min}=e_0^{side}}$ and $\sigma_{z0,FEM}^{side(b)}|_{e_{min}=ne_0^{side}}$ are used instead of the $\sigma_{z0,FEM}^{vtx(a)}|_{e_{min}=e_0^{vtx}}$ and $\sigma_{z0,FEM}^{vtx(b)}|_{e_{min}=ne_0^{vtx}}$, respectively, the λ_{side} is determined by the following equation.

$$\lambda_{side} = 1 - \frac{\ln\left(\sigma_{z0,FEM}^{side(a)}|_{e_{min}=e_0^{side}} / \sigma_{z0,FEM}^{side(b)}|_{e_{min}=ne_0^{side}}\right)}{\ln n} \quad (4)$$

Here, $\sigma_{z0,FEM}^{side(a)}|_{e_{min}=e_0^{side}}$ and $\sigma_{z0,FEM}^{side(b)}|_{e_{min}=ne_0^{side}}$ are the FEM stresses at the center $(0, -W/2, 0)$ on the interface end $y = -W/2$ in the finely and coarsely meshed 3D bonded plate models, respectively.

2.2. Mesh-independent technique useful for 3D bonded plate

The authors proposed the mesh-independent technique useful for 2D butt joint [3, 4]. The method is extended so that the ISSF at the vertex in 3D bonded plate can be analyzed. Figure 2 shows (a) unknown 3D bonded plate model and (b) reference 2D bonded plate model. The method for analyzing the ISSF K_{σ}^{vtx} at $(x, y, z) = (-W/2, -W/2, 0)$ in Fig. 2(b) by using the ISSF K_{σ}^{2D} at $(x, y) = (-W/2, 0)$ as the reference solution is mentioned below.

As shown in Fig. 2(a), the local polar coordinate (r, ϕ) is set at the vertex $(x, y, z) = (-W/2, -W/2, 0)$ in the 3D model. ϕ is the angle between the interface end $y = -W/2$ and r axis. When $\phi = \pi/4$, the singular stress field at $(-W/2, -W/2, 0)$ is expressed with the following equation [9].

$$\sigma_z^{vtx}(r, \phi = \pi/4) = \frac{K_{\sigma}^{vtx}|_{\phi=\pi/4}}{r^{1-\lambda_{vtx}}} \quad (5)$$

As shown in Fig. 2(b), the local polar coordinate (r, θ) is set at the interface end $(x, y) = (-W/2, 0)$ in the 2D model. θ is the angle between the interface end $y = 0$ and r axis. When $\theta = \pi/2$, the singular stress field at $(-W/2, 0)$ is expressed with the following equation [3, 4].

$$\sigma_y^{2D}(r, \theta = \pi/2) = \frac{K_{\sigma}^{2D}}{r^{1-\lambda_{2D}}} \quad (6)$$

The analysis methods focus average real/FEM stresses at and around the vertex. The FEM analyses are performed on the reference and unknown models under the similar mesh pattern. Since the mesh size dependency in the FEM stress is canceled by using a ratio, the average FEM stress ratio $\bar{\sigma}_{z,FEM}^{vtx}/\bar{\sigma}_{y,FEM}^{2D}$ corresponds to the average real stress ratio $\bar{\sigma}_z^{vtx}/\bar{\sigma}_y^{2D}$. When the stress in 3D model is averaged from $r = 0$ to $\sqrt{2}e_0^{vtx}$ and the stress in 2D model is averaged from $r = 0$ to e_0^{2D} , the following equation is obtained.

$$\frac{K_{\sigma}^{vtx}|_{\phi=\pi/4}}{K_{\sigma}^{2D}} = \frac{\lambda_{vtx}}{\lambda_{2D}} \cdot \frac{\sigma_{z0,FEM}^{vtx} \cdot (\sqrt{2}e_0^{vtx})^{1-\lambda_{vtx}} + \sigma_{z11,FEM}^{vtx} \cdot (\sqrt{2}e_0^{vtx})^{1-\lambda_{vtx}}}{\sigma_{y0,FEM}^{2D} \cdot (e_0^{2D})^{1-\lambda_{2D}} + \sigma_{y1,FEM}^{2D} \cdot (e_0^{2D})^{1-\lambda_{2D}}} \quad (7)$$

Here, $\sigma_{z11,FEM}^{vtx}$ is the FEM stress at $(r, \phi) = (\sqrt{2}e_0^{vtx}, \pi/4)$ in Fig. 2(a), $\sigma_{y0,FEM}^{2D}$ and $\sigma_{y1,FEM}^{2D}$ are the FEM stresses at $(r, \theta) = (0, \pi/2)$, $(e_0^{2D}, \pi/2)$ in Fig. 2(b), respectively.

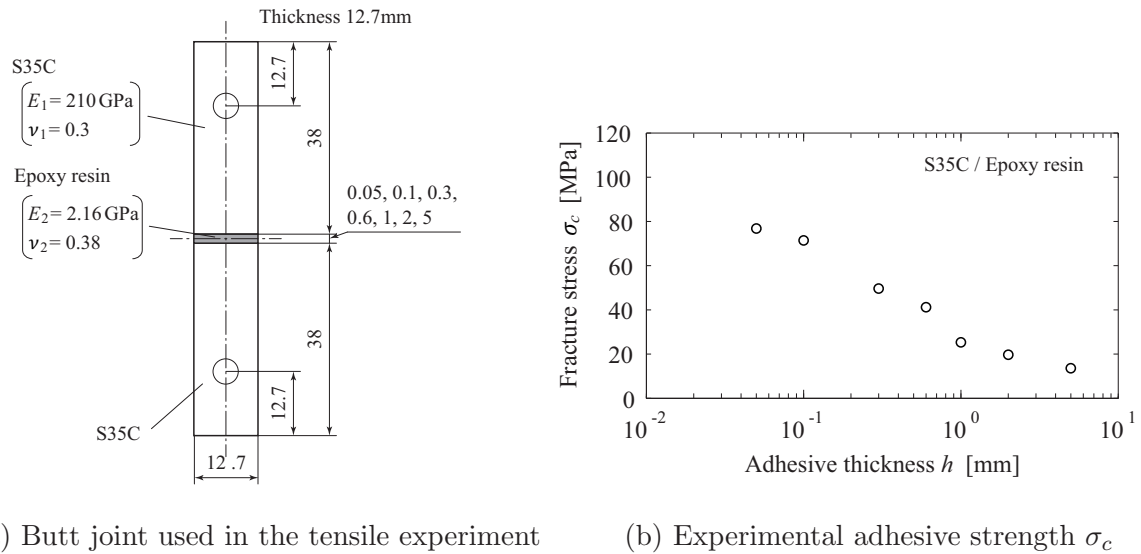
The local polar coordinate (r, ϕ) is set at the center $(0, -W/2, 0)$ in Fig. 2(b). ϕ is the angle between the interface end $y = -W/2$ and r axis. When $\phi = \pi/2$, the singular stress field at the center of interface end is expressed with the following equation [9]

$$\sigma_z^{side}(r, \phi = \pi/2) = \frac{K_{\sigma}^{side}|_{\phi=\pi/2}}{r^{1-\lambda_{side}}} \quad (8)$$

The following equation is obtained as well as Eq. (7).

$$\frac{K_{\sigma}^{side}|_{\phi=\pi/2}}{K_{\sigma}^{2D}} = \frac{\lambda_{side}}{\lambda_{2D}} \cdot \frac{\sigma_{z0,FEM}^{side} \cdot (e_0^{side})^{1-\lambda_{side}} + \sigma_{z01,FEM}^{side} \cdot (e_0^{side})^{1-\lambda_{side}}}{\sigma_{y0,FEM}^{2D} \cdot (e_0^{2D})^{1-\lambda_{2D}} + \sigma_{y1,FEM}^{2D} \cdot (e_0^{2D})^{1-\lambda_{2D}}} \quad (9)$$

Because the ISSF for 2D bonded plate by the body force method (BFM) [8, 10] is used, the ISSF for 3D bonded plate can be obtained by Eqs. (7) and (9) accurately.



(a) Butt joint used in the tensile experiment (b) Experimental adhesive strength σ_c

Figure 3. Schematic illustration of butt joint specimen and experimental adhesive strength [13, 14]

Table 1. Material properties used in the present analyses [13, 14]

Adherend (S35C)		Adhesive (Epoxy resin)		α	β	λ_{2D}	F_{σ}^{2D*}
E_1 [GPa]	ν_1	E_2 [GPa]	ν_2				
210.0	0.3	3.14	0.37	0.969	0.199	0.684	0.405

3. Debonding strength evaluation for butt joint by 3D model

The debonding strength for butt joint by 3D model is discussed by using the experimental result by Suzuki [14]. Figure 3 shows the schematic illustration of the butt joint specimen and the fracture stress. In the experiment, the adhesive thickness h is varied from 0.05 mm to 5 mm. The adherend is the low carbon steel JIS S35C. The adhesives are the epoxy resin. The fracture stress decreases with increasing h . Table 1 shows the material constants of the adherend and adhesives. Then, λ_{2D} and the dimensionless ISSF F_{σ}^{2D} for 2D bonded plate, which are used in the evaluation of the ISSF as the reference solution, are also shown in Table 1.

Analysis results in the case of $h = 5$ mm are mentioned as example below. Table 2 shows λ_{vtx} by Eq. (3) and λ_{side} by Eq. (4). λ_{side} nearly equals λ_{2D} . Table 3 shows the FEM stresses of unknown 3D butt joint model and reference 2D bonded plate model. All FEM stresses depend on the element size. However, it is found that the mesh size dependency can be overcome by multiplying the FEM stress by $(e_{min})^{1-\lambda}$. Therefore, the left-hand sides of Eqs. (7) and (9) have mesh size independency. Table 4 shows the ISSFs at the vertex by Eq. (7) and at the center by Eq. (9). It is found that K_{σ}^{vtx} and K_{σ}^{side} are independent of the element size. Figure 4 shows the singular stress distributions at the vertex and the center in the 3D butt joint model. The solid lines are the asymptotic solutions which are obtained by substituting the singular indexes in Table 2 and the ISSFs in Table 4 into Eqs. (5) and (8). The lines are in good agreement with the FEM stress distributions. The differences between the asymptotic solution and FEM stress are less than about 1% in $4.4 \times 10^{-6} < r/(W/2) < 7.89 \times 10^{-4}$ at the vertex and the center except for the nodes near the singular point which is strongly influenced by the singularity. It can be confirmed that the singular indexes and the ISSFs are determined accurately by the present method.

Figure 5 shows the critical ISSFs at the vertex and the center by 3D model and the critical

Table 2. Singular indexes λ_{vtx} by Eq. (3) and λ_{side} by Eq. (4)

(a) λ_{vtx}

Fine mesh model		Coarse mesh model		λ_{vtx}
e_0^{vtx}	$\sigma_{z0,FEM}^{vtx}$	e_0^{vtx}	$\sigma_{z0,FEM}^{vtx}$	
4.360×10^{-6}	89.49	1.744×10^{-5}	51.12	0.5961

(b) λ_{side}

Fine mesh model		Coarse mesh model		λ_{side}	λ_{2D}
e_0^{side}	$\sigma_{z0,FEM}^{side}$	e_0^{side}	$\sigma_{z0,side}^{side}$		
4.360×10^{-6}	36.02	1.744×10^{-5}	22.93	0.6741	0.6735

Table 3. Mesh-dependent FEM stresses of 3D butt joint model with $h = 5$ mm in Fig. 3 and reference 2D model under plane strain in Fig. 2(b)

(a) FEM stress at the vertex of unknown 3D butt joint model in Fig. 3

e_0^{vtx}	$\sigma_{z0,FEM}^{vtx}$	$\sigma_{z0,FEM}^{vtx} \cdot (e_0^{vtx})^{1-\lambda_{vtx}}$	$\sigma_{z11,FEM}^{vtx}$	$\sigma_{z11,FEM}^{vtx} \cdot (e_0^{vtx})^{1-\lambda_{vtx}}$
4.360×10^{-6}	89.49	0.6118	64.92	0.4438
1.744×10^{-5}	51.12	0.6118	37.09	0.4438

(b) FEM stress at the center of unknown 3D butt joint model in Fig. 3

e_0^{side}	$\sigma_{z0,FEM}^{side}$	$\sigma_{z0,FEM}^{side} \cdot (e_0^{side})^{1-\lambda_{side}}$	$\sigma_{z01,FEM}^{side}$	$\sigma_{z01,FEM}^{side} \cdot (e_0^{side})^{1-\lambda_{side}}$
4.360×10^{-6}	36.02	0.6453	27.87	0.4993
1.744×10^{-5}	22.93	0.6453	17.74	0.4993

(c) FEM stress at the interface end of reference 2D bonded plate model in Fig. 2(b)

e_0^{2D*}	$\sigma_{y0,FEM}^{2D*}$	$\sigma_{y0,FEM}^{2D*} \cdot (e_0^{2D*})^{1-\lambda_{2D}}$	$\sigma_{y1,FEM}^{2D*}$	$\sigma_{y1,FEM}^{2D*} \cdot (e_0^{2D*})^{1-\lambda_{2D}}$
3^{-12}	57.88	0.4399	44.79	0.3404
3^{-9}	19.73	0.4399	15.27	0.3404

Table 4. ISSFs for 3D butt joint with $h = 5$ mm

(a) K_{σ}^{vtx}			(b) K_{σ}^{side}		
e_0^{2D*}	e_0^{vtx}	K_{σ}^{vtx}	e_0^{2D*}	e_0^{side}	K_{σ}^{side}
3^{-12}	4.360×10^{-6}	0.392	3^{-12}	4.360×10^{-6}	0.418
3^{-12}	1.744×10^{-5}	0.392	3^{-12}	1.744×10^{-5}	0.418
3^{-9}	4.360×10^{-6}	0.392	3^{-9}	4.360×10^{-6}	0.418
3^{-9}	1.744×10^{-5}	0.392	3^{-9}	1.744×10^{-5}	0.418

ISSFs by 2D model [13]. $K_{\sigma c}^{side}$ almost equals $K_{\sigma c}^{2D}$. The $K_{\sigma c}^{vtx}$ is more constant against the thickness than that by 2D model and has the smallest scatter. The result can be never obtained

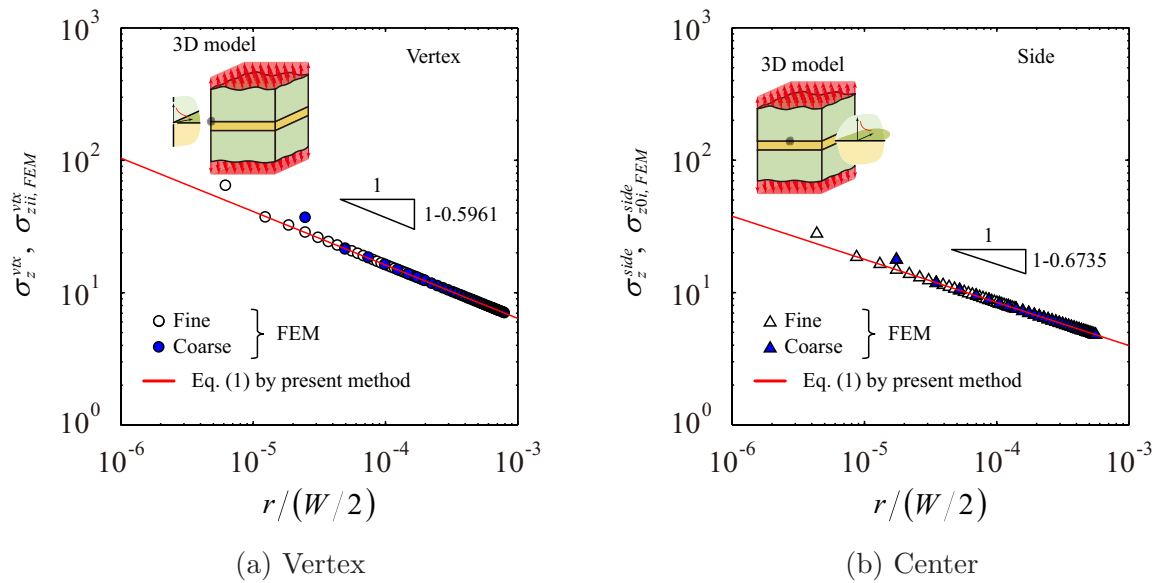


Figure 4. Singular stress distributions at the vertex and the center of butt joint with $h = 5$ mm

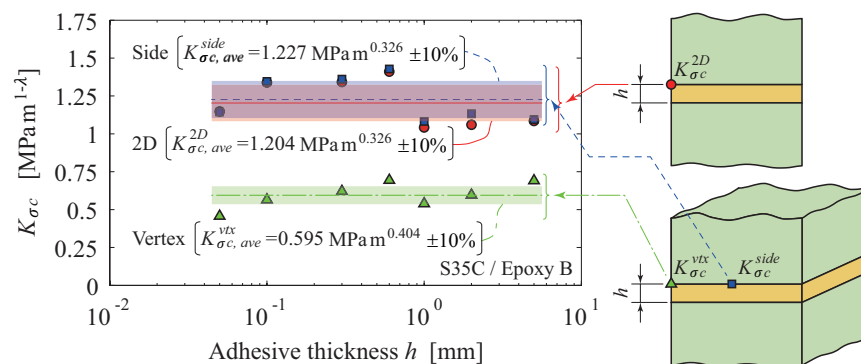


Figure 5. Relation between critical ISSF $K_{\sigma c}$ and adhesive layer thickness h

by 2D model.

4. Conclusion

In this paper, the practical analysis methods were proposed for analyzing the singular index and the intensity of singular stress field (ISSF) at the vertex of the interface in 3D bonded plate. The debonding strength for butt joint by 3D model is discussed by using the experimental result in the earlier study.

- (i) The critical ISSFs of the butt joints with various adhesive thicknesses in the earlier study were calculated by 3D and 2D models. The critical ISSFs at the center on the side in 3D model almost equaled those by 2D model. The critical ISSFs at the vertex in 3D model was less scattered than those at the center on the side in 3D model.
- (ii) The asymptotic solutions with the singular indexes and the ISSFs obtained by the present method were good agreement with the FEM stress distributions. The differences between the asymptotic solution and FEM stress were less than about 1% in $4.4 \times 10^{-6} < r/(W/2) <$

7.89×10^{-4} at the vertex and the center except for the nodes near the singular point which is strongly influenced by the singularity. It was confirmed that the singular indexes and the ISSFs are determined accurately by the present method.

References

- [1] Qian, Z. and Akisanya, A. R., An experimental investigation of failure initiation in bonded joints, *Acta Materialia*, Vol. 46, No. 14 (1998), pp. 4895-4904.
- [2] Mintzas, A. and Nowell, D., Validation of an H_{cr} -based fracture initiation criterion for adhesively, *Engineering Fracture Mechanics*, Vol. 80 (2012), pp. 13-27.
- [3] Zhang, Y., Noda, N. -A., Takaishi, K. -T., Lan, X., Effect of adhesive thickness on the intensity of singular stress at the adhesive dissimilar joint, *Journal of Solid Mechanics and Materials Engineering*, Vol. 4, No. 10 (2010), pp. 1467-1479.
- [4] Zhang, Y., Noda, N. -A., Wu, P. and Duan, M., A mesh-independent technique to evaluate stress singularities in adhesive joints, *International Journal of Adhesion and adhesives*, Vol. 57 (2015), pp. 105-117.
- [5] Noda, N. -A., Suryadi, D., Kumasaki, S., Sano, Y., Takase, Y., Failure analysis for coming out of shaft from shrink-fitted ceramic sleeve, *Engineering Failure Analysis*, Vol. 57 (2015), pp. 219-235.
- [6] Noda, N. -A., Chen, X, Sano, Y., Wahab, M. A., Maruyama, H., Fujisawa, R., Effect of pitch difference between the bolt-nut connections upon the anti-loosening performance and fatigue life, *Materials & Design*, Vol. 96 (2016), pp. 476-489.
- [7] Carpenter, W. C. and Byers, C., A path independent integral for computing stress intensities for V-notched cracks in a bi-material, *International Journal of Fracture*, Vol. 35 (1978), pp. 245-268.
- [8] Chen, D. H. and Nisitani, H., Intensity of singular stress field near the interface edge point of a bonded strip, *Transactions of the Japan Society of Mechanical Engineers, Series A*, Vol. 59, No. 567 (1993), pp. 2682-2686 (in Japanese).
- [9] Koguchi, H., Distribution of displacements and stresses near stress singularity field at a vertex in three-dimensional bonded structures, *Transactions of the Japan Society of Mechanical Engineers, Series A*, Vol. 66, No. 648 (2000), pp. 1597-1605 (in Japanese).
- [10] Noda, N. -A., Shirao, R. and Li, J., Sugimoto J. -S. Intensity of singular stress fields causing interfacial debonding at the end of a fiber under pullout force and transverse tension, *International Journal of Solids and Structures*, Vol. 44 (2007), pp. 4472-4491.
- [11] Miyazaki, T., Noda, N. -A., Evaluation of debonding strength of single lap joint by the intensity of singular stress field, *Journal of Physics: Conference Series*, Vol. 842 (2017), pp. 012078.
- [12] Miyazaki, T. , Noda, N. -A., Ren, F., Wang, Z., Sano, Y., Iida, K., Analysis of intensity of singular stress field for bonded cylinder and bonded pipe in comparison with bonded plate, *International Journal of Adhesion and Adhesives*, Vol. 77, (2017), pp. 118-137
- [13] Noda, N. -A., Miyazaki, T., Li, R., Uchikoba, T. and Sano, Y., Debonding strength evaluation in terms of the intensity of singular stress at the interface coner with and without fictitious crack, *International Journal of Adhesion and adhesives*, Vol. 61 (2015), pp. 46-64.
- [14] Suzuki, Y., Adhesive tensile strengths of scarf and butt joints of steel plates (Relation between adhesive layer thicknesses and adhesive strengths of joints), *JSME International Journal*, Vol. 30, No. 265 (1987), pp. 1042-1051.